Low Profile Fully Planar Folded Dipole Antenna on a High Impedance Surface

Andrea Vallecchi, Javier R. De Luis, *Member, IEEE*, Filippo Capolino, *Senior Member, IEEE*, and Franco De Flaviis, *Senior Member, IEEE*

***Abstract*—A fully planar antenna design incorporating a high impedance surface (HIS) is presented. The HIS is composed by a periodic array of subwavelength dogbone-shaped conductors printed on top of a thin dielectric substrate and backed by a metallic ground plane. First, the characteristics of a dipole over PEC or PMC layers, a dielectric slab, and the HIS are compared and studied in detail, highlighting the advantages provided by the use of the HIS. Then, the design of a low profile folded dipole antenna working at 5.5 GHz on top of the HIS is described. The surface provides close to 6% antenna impedance bandwidth and increased gain up to 7 dBi, while shielding the lower half space from radiation. The antenna structure comprises three metal layers without any vias between them, and its overall thickness is $0.059\lambda_0$. The dipole is fed by a balanced twin lead line through a balun transformer integrated in the same antenna layer. A prototype has been built and measurements confirming simulation results are provided.**

***Index Terms*—AMC ground plane, artificial magnetic conductor, artificial magnetism, artificial substrate, impedance surface, low profile antenna, metamaterials, reflection phase.**

I. Introduction

SINCE the advent of electromagnetic bandgap (EBG) materials and metamaterials, researchers have tried to realize artificial magnetic conductors (AMCs) [1]–[5] that can provide an effective shielding of radiation without requiring the vanishing of the tangential electric field. One important application of AMCs is, for example, as the ground plane of an electric dipole for a low profile design with increased forward directivity [6]–[13]. In this context, according to different terminologies in use, the metamaterial surface is denoted either as EBG ground plane [7], [8], [10], [14], reactive impedance substrate [9], magnetic ground plane, or high impedance surface (HIS) [5].

Manuscript received September 03, 2010; revised May 17, 2011; accepted June 21, 2011. Date of publication September 15, 2011; date of current version January 05, 2012. This work was supported in part by the Semiconductor Research Cooperation (SRC)-GRC under Grant 2009-VJ-1962.

A. Vallecchi was with the Department of Electrical Engineering and Computer Science, University of California-Irvine, Irvine, CA 92697 USA. He is now with the Department of Information Engineering, University of Siena, 53100 Siena, Italy (e-mail: andrea.vallecchi@unisi.it).

J. R. De Luis, F. Capolino, and F. De Flaviis are with the Department of Electrical Engineering and Computer Science, University of California-Irvine, Irvine, CA 92697 USA (e-mail: jrodrig2@uci.edu; f.capolino@uci.edu; franco@uci.edu).

Color versions of one or more of the figures in this paper are available online at http://ieeexplore.ieee.org.

Digital Object Identifier 10.1109/TAP.2011.2167912

High impedance surfaces have been initially realized by using "mushroom" type structures [1], [7], [14], [15] requiring a ground plane and multiple metallic vias. However, some authors have suggested that the presence of vias could produce distortion of the radiation pattern within the operating band [10]. In this work an artificial reactive impedance surface is realized using a periodic structure printed on a planar grounded substrate without any via. This structure is similar to the one presented in [5] though its modeling is substantially different since in this case a subwavelength thickness is used for the dielectric layer.

Recently, a planar metamaterial consisting of paired metallic conductors with dogbone shape was shown to support symmetric (electric) and antisymmetric (magnetic) resonance modes. The antisymmetric mode, also referred to as transmission line mode, has been demonstrated to be associated with artificial magnetism [11]–[13], [16]–[18]. In accordance with image theory, the magnetic resonance can be obtained by using a single layer of dogbones over a perfect electric conductor (PEC) plane, therefore reducing by half the required thickness of the HIS with respect to the basic configuration in [13]. The proposed structure does not require any via between its constituent layers and can be entirely fabricated in planar technology [19], [20].

Along the lines of the design reported in [19], the HIS is used in this work to enhance the bandwidth and directivity performance of a printed dipole, located very close to an underneath metallic ground plane. The proposed antenna consists of a three metal layer structure. The top layer allows the placement of any planar radiating element or array that can benefit from the properties of the HIS. The intermediate layer accommodates the periodic metallic dogbone-like patterned surface that constitutes the metamaterial, whereas the bottom layer serves as a sheltering ground plane. The design is centered within the 5-GHz band for WiFi/WLAN applications.

The organization of the paper is the following. In Section II, different designs of a low profile dipole antenna placed either on top of PEC and PMC layers or a dielectric slab are analyzed in order to highlight the advantages of using a HIS. Then, in Section III, the fully planar HIS with subwavelength thickness and its effective transmission line model are presented. Section IV describes the design of a low profile folded dipole on top of the proposed HIS. Simulations and measurements are presented in Section V. Finally, the influence of the HIS size on the dipole antenna performance are numerically investigated in Section VI.

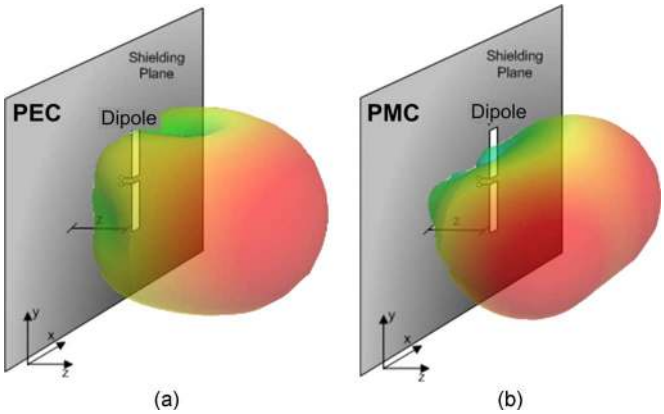

Fig. 1. 3D radiation patterns of a strip planar dipole operating at 5.5 GHz at a distance $0.03\lambda_0$ from (a) PEC and (b) PMC layers with size $1\lambda_0 \times 1\lambda_0$. Red and green colors indicate strong and weak field intensity, respectively.

II. Analysis of Different Low Profile Antenna Design Approaches

In order to understand the benefits of using a HIS, different designs of a low profile dipole antenna are compared in a comprehensive manner.

We first consider the cases when a dipole is placed at a certain small electrical distance z above a PEC or PMC plane, as shown in Fig. 1(a) and (b), respectively. Although PMC materials do not exist in nature, this design is considered for comparative purposes.

The enhancement of the antenna directivity for the dipole over the PEC surface is larger than for the PMC case, as shown in Fig. 1. However, other important antenna parameters are differently affected by the presence of the PEC or PMC reflecting surfaces as discussed next, and compared to the performance of a dipole over a HIS, discussed in the next sections.

A simulation experiment is conducted with HFSS to understand the behavior of a strip dipole located close to a PEC or PMC layer. In Fig. 2 the distance z between a dipole with length $0.45\lambda_0$ and a PEC plane with area $1\lambda_0 \times 1\lambda_0$ is increased from $0.01\lambda_0$ to $0.5\lambda_0$, where λ_0 denotes the free space wavelength at 5.5 GHz. Fig. 2(a) shows the input impedance as a function of the dipole distance from the PEC or PMC plane. When the dipole approaches the plane, the input resistance decreases considerably for the PEC case (the dipole and image currents cancel each other), whereas it reaches the largest value for the PMC case (the dipole and image currents add up in phase). On the other hand, when the distance of the dipole from the reflecting surface is larger than $0.5\lambda_0$ the input impedance starts to be comparable with the free space values for both the PEC and PMC cases.

The directivity of the dipole at small distances from the conducting plane, shown in Fig. 2(b), is at least 3 dBi higher for the PEC surface compared to the PMC case. This is also confirmed by the shape of the radiation patterns shown in Fig. 1 when the dipole is just $0.03\lambda_0$ above the PEC or PMC plane.

From this experiment we can outline some important considerations upon the design aspects of a low profile dipole above a PEC plane:

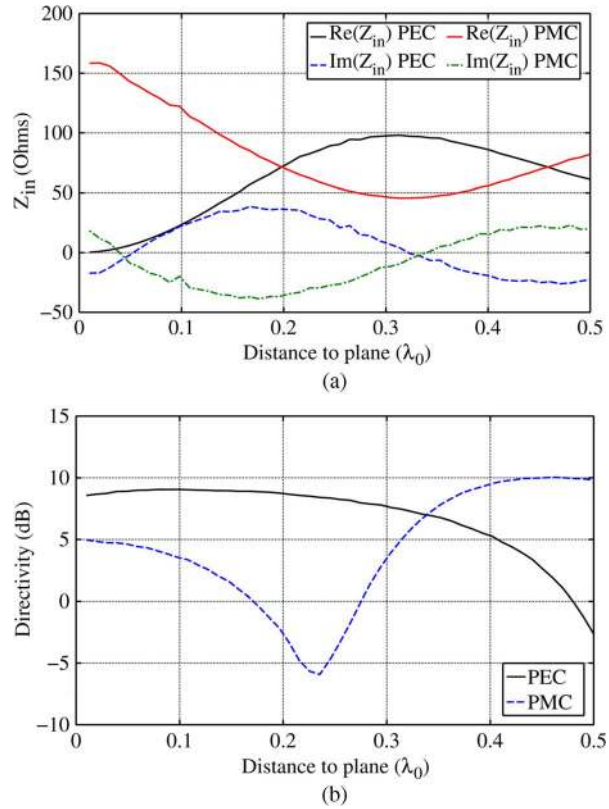

Fig. 2. (a) Input impedance and (b) forward directivity of a dipole working at 5.5 GHz versus the dipole separation distance from a PEC or PMC finite ground plane with size of $1\lambda_0 \times 1\lambda_0$.

(a) The low radiation resistance (comparable in some cases to the loss resistance) implies that in a system with losses, the antenna radiation efficiency decreases considerably. Besides, impedance matching the antenna to a 50 Ohm system will become increasingly more difficult as the distance of the dipole from the reflecting surface is reduced.

(b) The energy stored in the near field of the dipole will be large, producing an antenna with a high Q (defined as the ratio of energy stored to energy accepted by the antenna [21]) and, correspondingly, with a very narrow impedance bandwidth.

The last point is ultimately the main bottleneck of using a dipole over a PEC plane for most practical applications.

On the other hand, the impedance value for the low profile dipole over the PMC layer seems more favorable from the antenna matching point of view, but in this case the radiation pattern does not show the desired directivity enhancement.

A folded dipole could be used over the PEC plane in place of the regular dipole, as suggested in [21], to increase the input resistance of the antenna and achieve a better impedance matching. The reflection coefficient and input impedance for a folded dipole with length of $0.45\lambda_0$ located above a PEC plane are compared with the corresponding quantities for the regular dipole over PEC and PMC planes in Fig. 3 and Fig. 4, respectively. The reflection coefficient (dashed line) in this case is below -12 dB at 5.45 GHz. Even though matching can be improved by using a folded dipole, the disadvantage of a narrow impedance bandwidth (2.75% at the level of -10 dB) is still present, as apparent from Fig. 3.

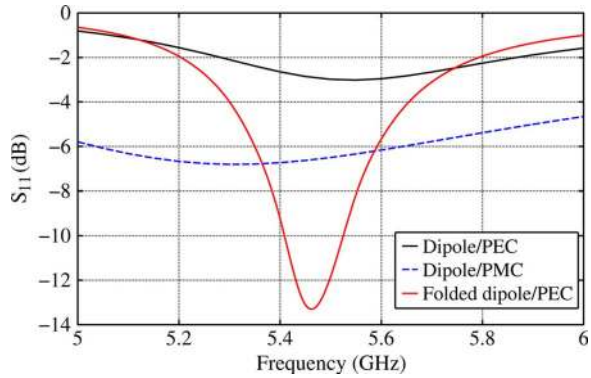

Fig. 3. Reflection coefficient for different dipole antenna configurations: regular dipole of length $0.45\lambda_0$ (5.5 GHz) in front of a PEC layer (solid black line); regular dipole in front of a PMC layer (dashed blue line); folded dipole with length $0.45\lambda_0$ (5.5 GHz) in front of a PEC plate (solid red line). In all cases, the antenna is placed at a distance of 3.22 mm $(0.059\lambda_0)$ away from the PEC plate, whose size $1\lambda_0 \times 1\lambda_0$.

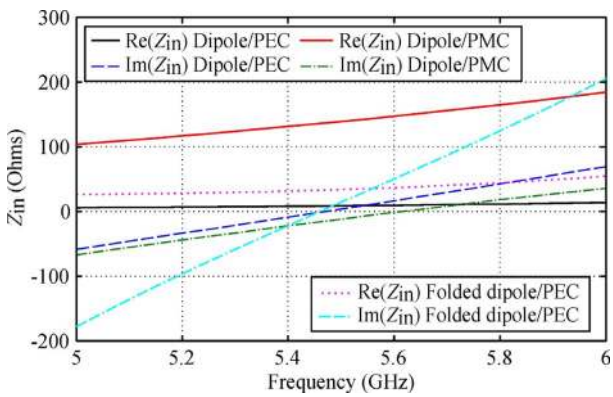

Fig. 4. Input resistance and reactance corresponding to the three different antenna configurations considered in Fig. 3.

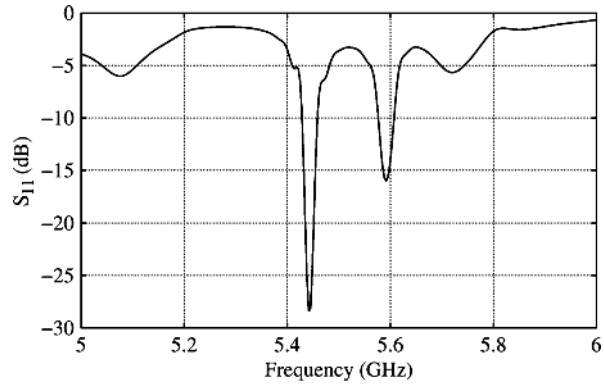

Fig. 5. Magnitude of the reflection coefficient of a dipole of length $0.385\lambda_0$ on top of a grounded dielectric slab with dielectric permittivity $\varepsilon_r = 25$, thickness $0.03\lambda_0$ and area $1\lambda_0 \times 1\lambda_0$.

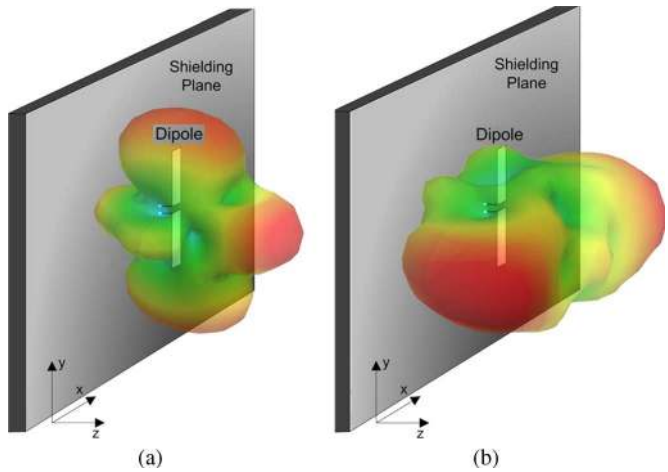

Fig. 6. 3D radiation pattern at 5.44 GHz (a), 5.58 GHz. of the dipole with reflection coefficient shown in Fig. 5. Red and green colors indicate strong and weak field respectively. The dipole is placed (printed) on top of a dielectric stub of thickness $0.03\lambda_0$.

In order to design a low profile dipole one could also think of placing the dipole on top of a high permittivity dielectric slab backed by a metallic conductor plane. Besides yielding to small thicknesses because of a smaller effective wavelength in the dielectric substrate, this results also in a shorter dipole length $(0.385\lambda_0)$. The drawback is that the high permittivity substrate supports surface waves that can trap a significant amount of power emitted by the antenna and become the main radiation mechanism, which distorts the dipole radiation pattern. In this scenario, the patterns become of the endfire type, as the surface waves will diffract at the substrate edges and radiated into space. In addition, if the waves are propagating in a lossy substrate, the radiation efficiency will drop resulting in a low gain antenna.

Fig. 5 shows the reflection coefficient of a dipole of length $0.385\lambda_0$ on top of a grounded dielectric slab with relative permittivity $\varepsilon_r = 25$, thickness $0.03\lambda_0$ and size $1\lambda_0 \times 1\lambda_0$. The effect of the dielectric slab is to provide two different resonances at 5.44 GHz and 5.58 GHz. The pattern associated with these resonances corresponds to a surface wave radiated in the y (Fig. 6(a)) and x direction (Fig. 6(b)), respectively. Therefore, the patterns become of the endfire type, and the dipole merely acts as the source for the surface wave propagation that will be diffracted at the substrate edges and radiated into space.

III. High Impedance Surface

From the discussion in the previous section, it is clear that the PEC, PMC and dielectric slab cases are complementary in terms of advantages. While the PEC ground plane provides a directive broadside pattern but suffers from high quality factor and narrow impedance bandwidth, the ideal PMC surface shows improved bandwidth but lower directivity. On the other hand, a high dielectric permittivity substrate results in most of the power emitted by the dipole being trapped in the substrate. A HIS can combine the advantages of both PEC and PMC ground planes. In fact, a proper HIS design can achieve an improved bandwidth with respect to the PEC case and higher forward directivity with respect to the PMC case.

Fig. 7 shows the developed HIS design, that is formed by a doubly periodic array of dogbone-shaped conductors printed on a grounded dielectric substrate with thickness $H = 1.61$ mm (dielectric plus copper thickness), relative dielectric constant $\varepsilon_r = 2.2$, and $\tan\delta = 0.0009$ (e.g., RT/Duroid 5880). The various geometrical parameters characterizing the unit cell of this metamaterial (Fig. 7(b)) are as follows (in mm): $A = 7$, $B = 7$, $A1 = 0.875$, $B1 = 3.5$, $A2 = 6.83$, $B2 = 0.7$, $H = 1.61$. The thickness of the copper metal layers is 35 μm. The total

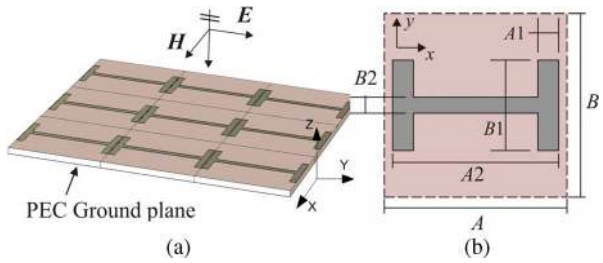

Fig. 7. (a) HIS composed of a doubly-periodic array of dogbone-shaped conductors printed on a PEC-backed dielectric material. (b) Unit cell of the HIS with indication of geometrical parameters.

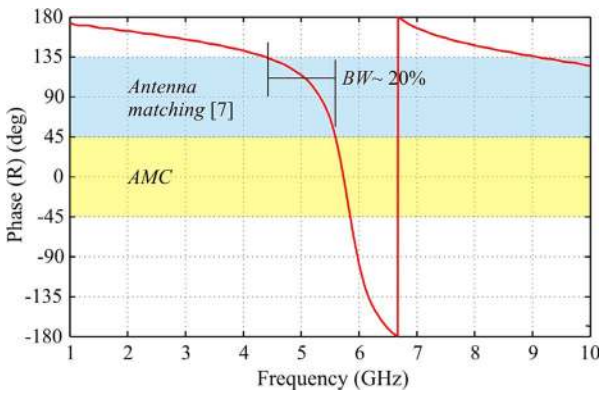

Fig. 8. Phase of the reflection coefficient calculated from CST full-wave simulations, de-embedded at the level of the top dielectric layer, (where the dipole antenna will be located), $z = 3.2$ mm away from the bottom ground plane, for a plane wave normally incident as shown in Fig. 7(a).

number of dogbones constituting the surface is 30 (5×6 unit cells) which gives a total surface area of 34.8×38.5 mm^2. The presence of an additional dielectric layer (1.61 mm thick) covering the dogbone metallic array, which is required to support the dipole is taken into account in the design and simulations.

The principle of operation of HISs can be understood from the interpretation of the following two important characteristics.

i) The phase of the reflection coefficient (Fig. 8) that the surface presents at normal incidence, expressed as

$$\angle R = \text{ang}\left\{\frac{Z_A - Z_0}{Z_A + Z_0}\right\}. \quad (1)$$

ii) The value of normalized surface reactance versus frequency, defined as $jX_A = Z_A/Z_0$.

The magnitude of the reflection coefficient is related to the dielectric and conductor losses, and can be significantly smaller than unity for certain patterned conductor geometries and for thin substrates. However, for the present application, the HIS configuration involves minimal losses and $|R| \approx 1$. Therefore, either the phase of R or X_A can be used to characterize the HIS response. The behavior of these types of surfaces has been analyzed at oblique incidence [5] and different incident polarizations [7]. For the application considered here, we will limit our analysis to the case of normal incidence and linear polarization.

Fig. 8 shows the phase of the reflection coefficient for this surface (assumed with infinite transverse extent) where the reference plane has been de-embedded up to the dielectric cover at to the point $z = 3.2$ mm where the antenna will be located. The so called magnetic resonance frequency [13] is very close to the frequency where the reflection phase value reaches zero degrees and the surface behaves as an AMC. For this specific dogbone geometry, the magnetic frequency is designed to occur at $f_m \approx 5.8$ GHz. Below and above this frequency the reactance becomes inductive and capacitive, respectively. When the asymptote of the phase tends to ± 180 degrees, the surface substantially behaves as a PEC. The position of the magnetic frequency can be controlled through different design parameters, such as the substrate thickness and permittivity, and the shape of dogbone conductors, as described in [12], [13], [18]. Approximate formulas for its evaluation can be found in [13].

In the intermediate states between the AMC and PEC behaviors, the surface exhibits a reactance X_A that is either capacitive or inductive, and near the resonance frequency presents a high impedance value. Therefore, the surface can be more generally referred to as a HIS [9]. As a result of this behavior, placing a dipole on top of a HIS can provide improved impedance matching, bandwidth enhancement, and increased forward directivity due to the total reflection properties of the reactive surface (the reflection coefficient has a unity magnitude, as previously pointed out). In addition, below the magnetic resonance the HIS exhibits an inductive reactance that can compensate for the capacitive reactance of a dipole below its natural resonant frequency. As a consequence, the resonance of the dipole can be achieved at a lower frequency than its resonant frequency in free space, resulting in some degree of antenna miniaturization, as stated in [9].

An important question arises. Which is the frequency range where a HIS can be more effectively used? Some authors argue that it could be advantageous in terms of antenna impedance matching to work in the region where the phase of the reflection coefficient is 90 $\pm$ 45 degrees (i.e., the inductive region) [7], [9]. The authors of [7] conclude with a parametric analysis where it is shown that the operative HIS bandwidth increases with the smoothness of the phase reflection in the transition region. In general one could classify and rank the performance of any HIS by using this factor as a figure of merit. However, other authors have used different operation regimes beyond the magnetic frequency to realize low profile antennas with total thickness below $0.06\lambda_0$ [10], [15] without apparent pattern degradation and VSWR < 2 within the operative band. One of the most relevant conclusion of these studies is that the HIS operative bandwidth must be considered together with the antenna design and not as an independent property valid for all antenna cases. After all, [7], [10], [15] seem to agree that the operative bandwidth definition for HISs needs to consider radiation pattern bandwidth as well as impedance bandwidth characteristics simultaneously.

IV. Low Profile Antenna Over a High Impedance Substrate

A. Dipole over HIS

A copper planar dipole is now placed on top of the HIS to compare with the scenarios previously presented.

The length of the printed dipole antenna is assumed as a variable parameter, whereas the dipole width is fixed to 1 mm

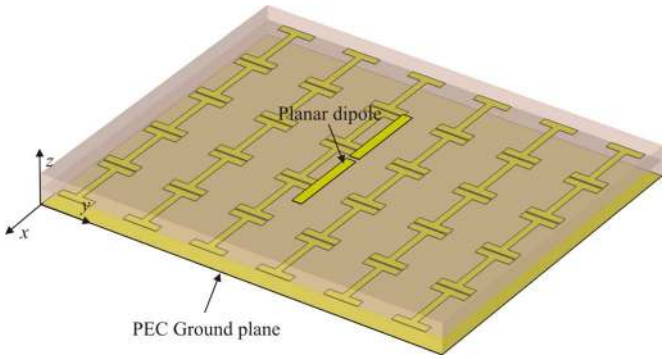

Fig. 9. Planar dipole antenna placed at 1.61 mm $(0.0295\lambda_0)$ above the HIS. The total thickness of the antenna (including the dipole, the copper thickness and the dogbone substrate) is 3.22 mm $(0.059\lambda_0)$.

$(0.018\lambda_0)$. Fig. 9 shows the dipole over the HIS, which is excited using an ideal lumped port source between its arms. The height of the dipole above the HIS including copper thickness (i.e., the dogbone metal layer) is 1.61 mm $(0.0295\lambda_0)$ and thus, the total thickness of the antenna (including the dipole, the copper thickness and the dogbone grounded substrate) is 3.22 mm $(0.059\lambda_0)$.

For a practical and planar realization of the feed, a twin line with characteristic impedance of approximately 112 Ohm will be used (a lower resistance would require the use of very wide twin line conductors, whose spurious radiation could deteriorate the antenna radiation pattern, and/or a gap between the line conductors smaller than 0.2 mm which would be difficult to be reliably realized by simple lithographic techniques). Therefore, the dipole needs to exhibit a similar input impedance at its terminals to achieve a good impedance matching and low reflection coefficient.

The simulated input resistance and reactance of the dipole for several dipole lengths are shown in Fig. 10(a) and (b), respectively. The length of the dipole is expressed in terms of the wavelength in the dielectric substrate, λ_d, as $L = x\lambda_d$, with x varying over the values 0.48, 0.5, 0.52, 0.54. The dipole input resistance exhibits much lower values than 112 Ohm at the desired frequency of operation (5.5 GHz). It is however higher than the 8 Ohm of the regular dipole at the same distance from a PEC plane as seen in Section II. Increasing the dipole length, we can obtain slightly higher resistance values at the expense of a higher reactance, which makes the matching more critical. Different center locations of the dipole were also simulated to test whether this could have any influence on the input resistance. In particular, instead that placing the dipole between two rows of dogbones, i.e. above a non-patterned portion of the HIS as in Fig. 9, the dipole aligned with one dogbone row has been simulated, with its center either between two adjacent dogbones, or right over a dogbone center. It was found that both of these alternative dipole center locations indeed yield a higher input resistance, but unfortunately also a steeper variation of the input reactance, so that the matching to the twin line impedance can be only accomplished over a very narrow frequency band.

Therefore, if the overall antenna profile is not to be increased (and the target is to keep a low profile), another type of antenna able to provide a higher input resistance is desirable. It is well

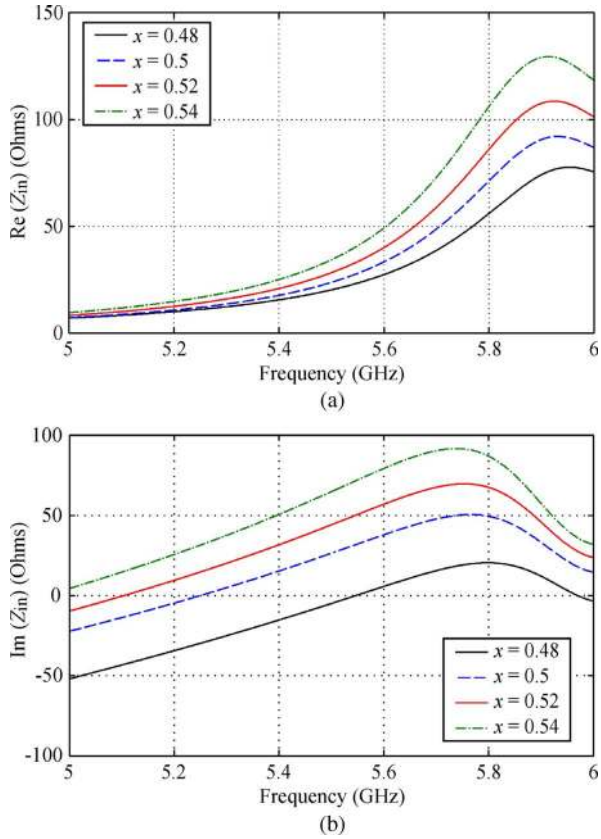

Fig. 10. (a) Input resistance and (b) input reactance for several dipole lengths $L = x\lambda_d, x = 0.48, 0.5, 0.52, 0.54$. The dipole is placed $0.0295\lambda_0$ (1.61 mm) above the HIS, which is printed on a dielectric substrate with permittivity $\varepsilon_r = 2.2$ and $\tan\delta = 0.0009$.

known that folded dipole antennas resonate with an input resistance about four times larger than that of a regular dipole [22]. At the same time, a folded dipole presents a larger impedance bandwidth (17% simulated in free-space) than a single dipole (typically 10% in free-space) due to the fact that the folded arm helps to smooth the behavior of the input reactance with frequency. A larger resistance than in Fig. 10(a) could be by itself a good starting point for a low profile antenna to achieve good matching to a twin line. Therefore this design approach is developed next.

B. Printed Folded Dipole Over HIS

A folded dipole antenna with overall length of 17.25 mm $(\sim 0.3\lambda_0)$, gap between arms of 1 mm $(0.018\lambda_0)$, and strip width of 1 mm, as depicted in Fig. 11, has been designed to work at 5.5 GHz. The dipole is excited by a twin line with conductor width of 1 mm, gap between conductors of 0.2 mm, and a simulated characteristic impedance of $\sim$112 Ohm.

Further miniaturization of the surface can be accomplished (cf. Section VI), though not attempted here in this first fully planar realization. The folded dipole is placed on top of the designed HIS surface. Its reflection coefficient is plotted in Fig. 12 and compared to that obtained when the dogbone array is removed (i.e., dipole on top of a 3.22 mm thick RT/Duroid-5880 dielectric substrate backed by a copper ground plane only). The folded dipole over the HIS fed by the twin line presents a good

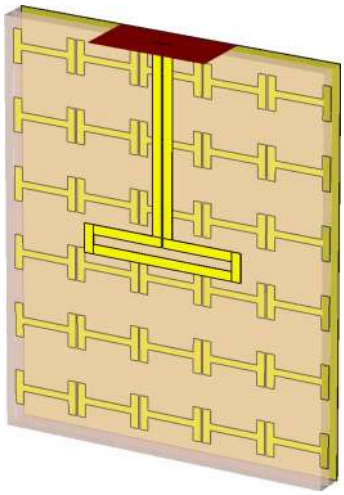

Fig. 11. A folded dipole antenna with length of 17.25 mm ($0.316\lambda_0$), gap between arms of 1 mm ($0.018\lambda_0$), and strip width of 1 mm. The antenna is 1.61 mm away from the HIS and is designed to behave as AMC at 5.5 GHz.

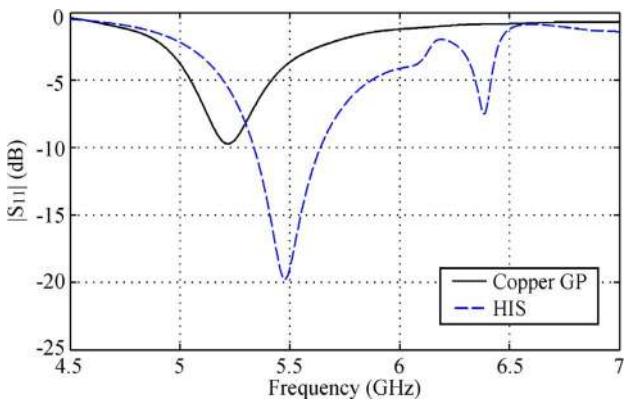

Fig. 12. Reflection coefficients of the folded dipole with length $0.3\lambda_0$ over a copper ground plane (solid black line) and the HIS (dashed blue line). The overall thickness for both structures is equal to $0.059\lambda_0$.

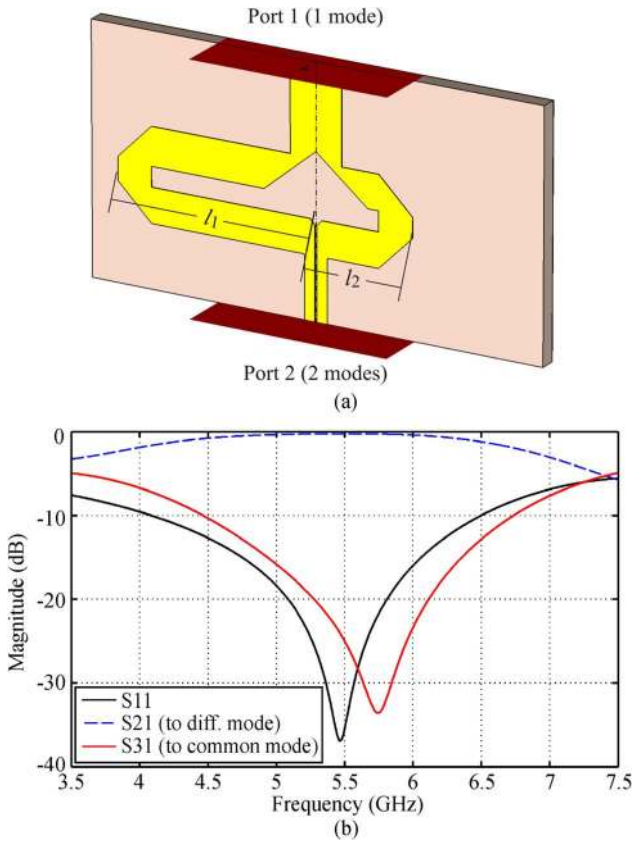

Fig. 13. (a) Wilkinson balun designed to transform the unbalance microstrip transmission line (port 1) to the balance twin lead transmission line (ports 2 and 3). The structure is printed on RT/Duroid 5880 with $\varepsilon_r = 2.2$ and $\tan\delta = 0.0009$. (b) Magnitude of the reflection coefficient, common mode rejection and differential mode transmission of the proposed Wilkinson balun.

impedance matching condition at the desired frequency and a fractional bandwidth of about 6%. This value is higher than the 2.75% of the folded dipole at the same distance from a PEC plane as seen in Section II. If gain-bandwidth enhancement is the primary design objective, the choice of the final antenna shape and overall stack up profile may be helped by the use of optimization algorithms as shown in [8].

C. Printed Balun Design

When a balanced dipole antenna is fed by a twin line and directly connected to an unbalanced transmission line such as a coaxial cable, currents will flow on the coaxial outer conductor producing pattern distortion due to spurious radiation from the feed. A balance to unbalanced transformer or balun is typically used to mitigate this problem.

A balun suppresses the common mode current in the dipole arms. Some types of balun also provide input/output impedance transformation. Many approaches for balun realizations are reported in the literature [23]. In this paper, due to the desired low-profile characteristic, a microstrip-to-coplanar strips transition consisting of a symmetric T-junction [24] followed by a 180° delay line [25] is printed on the same layer as the folded dipole, as shown in Fig. 13(a). This balun structure was shown to feature broadband, low reflection coefficient. The ground plane for the balun is placed on the intermediate dogbone layer (Fig. 14). Though this balun is quite large, due to the low permittivity of the substrate (which, for simplicity, is the same of the dipole) and tends to affect the antenna radiation performance, it is needed here for antenna measurements via coaxial cables. Nevertheless, it can be considered as an external module rather than part of the antenna, and it could be realized in a more compact form using another type of substrate or different technology.

In Fig. 13, the input port 1 is the microstrip unbalanced transmission line, with characteristic impedance $Z_c = 50\ \mathrm{Ohm}$, where the SMA connector will be soldered. At the output port, we have three separated conductors, and thus two different and not degenerated quasi-TEM modes can be supported. The even and odd mode of the coupled output microstrips represent these two physical modes that can travel along the line. Both these modes are considered in the simulation. The even mode has a characteristic impedance $Z_{c1} = 110\ \mathrm{Ohm}$, whereas the common mode has a characteristic impedance $Z_{c2} = 80\ \mathrm{Ohm}$. The power coming from port 1 is split into two different paths. The balun is designed to introduce 180 degrees of phase delay between the two microstrip line branches by adjusting their

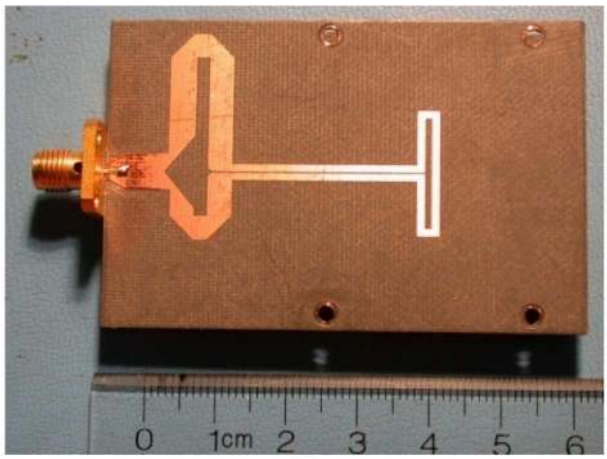

(a)

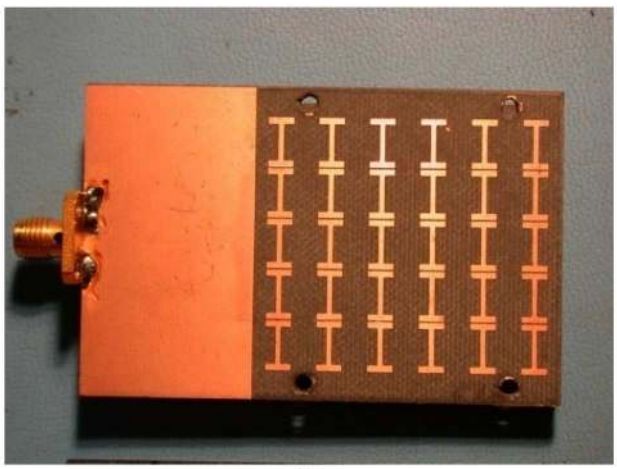

(b)

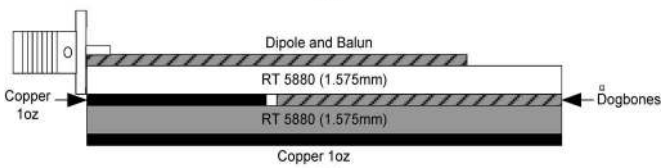

(c)

Fig. 14. Fully planar realization of a low profile dipole antenna on top of a HIS. (a) Top metal layer with a folded dipole and a balun from the unbalanced microstrip feed line to the balanced twin line. (b) Intermediate metal layer (on the opposite side of the dipole substrate) showing the ground plane for the balun and the dogbone layer under the folded dipole. The dogbones are then located on top of a grounded substrate, as shown in (c), the cross-sectional view of the layer stackup.

lengths so that $l_1 - l_2 \approx \lambda_g/4$, where $l_{1,2}$ are the lengths of the two branches as in Fig. 13(a), and λ_g is the guided wavelength in the microstrip. By doing this, the propagation mode in the coupled output microstrips will be dominantly the odd mode, which is tightly bound to the pair of line conductors and can be easily transferred into the differential twin line mode after the ground plane in the intermediate layer of the dielectric stack is truncated. To reduce undesired reflection and radiation losses at the 90-degree microstrip bends, optimal miters have been employed [26]. As a result, the good reflection coefficient (S_{11}) and common mode rejection characteristics (S_{31}) shown in Fig. 13(b) have been obtained. Indeed, the common mode rejection is larger than 20 dB, while the differential mode

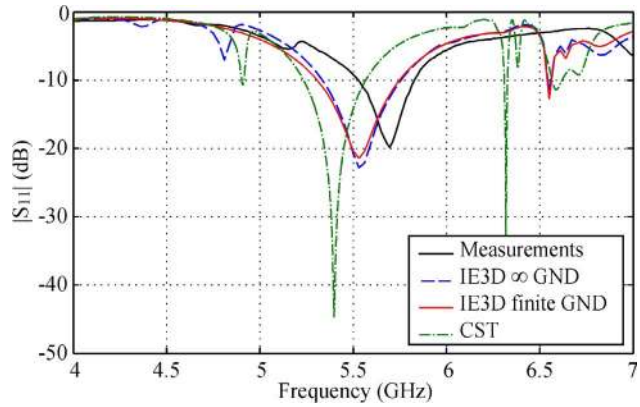

Fig. 15. Simulated and measured reflection coefficient at the antenna connector (see Fig. 14). Simulations are performed with CST Microwave Studio and IE3D, taking into account the finite thickness of metal layers (35 μm). In IE3D the dielectric layers are assumed to be of infinite extent, whereas both the cases of infinite and finite-size ground plane have been simulated. The IE3D mesh is made by approximately 20 subdomain divisions per wavelength (at a frequency of 7 GHz).

transmission (S_{21}) is close to 0 dB. Moreover, the operative bandwidth of the balun (∼36%) is much larger than the simulated impedance bandwidth of the folded dipole.

V. Simulated and Measured Results of a Folded Dipole With Balun Over His

Once the folded dipole is connected to the balun, the design is complete, and ready for fabrication and measurements. For the fabrication of the prototype we have used RT/Duroid 5880 laminates, with $\varepsilon_r = 2.2$ and $\tan\delta = 0.0009$, and 35-μm-thick copper foils. The two faces of the antenna top layer, containing the dipole with its feed, on the upper side, and the ground of the dipole feed as well as the dogbone array, on the lower side, are illustrated in Fig. 14(a) and (b), respectively, whereas a sketch of the antenna cross-section is depicted in Fig. 14(c).

The reflection coefficient of the prototype was measured using an HP8510C vector network analyzer and is compared with simulation results in Fig. 15. Good agreement is observed between the numerical results obtained by using two completely different EM simulators, one based on the finite integration technique in time domain (CST Microwave Studio), and the other on the method of moments (IE3D from Zeland).

The simulations with IE3D are carried out using an infinite as well as a finite ground plane (in Fig. 15, dashed blue and red curves, respectively), whereas the dielectric layers are assumed to be of infinite extent. Differently, the simulations with CST also take into account the finiteness of the dielectric substrates. In both CST and IE3D, metal layers are modelled with their actual finite thickness. All simulations and measurements show that at the center frequency the magnitude of the reflection coefficient is as low as -20 dB. Anyway, it is noted that the prediction by IE3D is closer to the measured data in terms of both the resonance frequency and reflection coefficient value. The small frequency shift between simulations and measurements may be due to fabrication tolerances. 35 μm thick (1 oz) foil rolled copper (RT/Duroid 5880) was used and a 40 μm thick photoresist laminate was placed on top to make the board photosensitive. However, the space between the twin lines is 200 μm

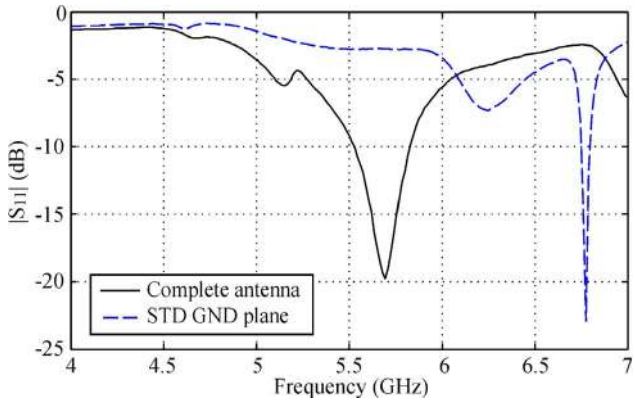

Fig. 16. Measured reflection coefficient response for the complete antenna structure including the HIS ("Complete antenna"), and the structure where the dogbone layer is replaced by a solid ground plane ("STD GND plane").

and between contiguous dogbones is just 170 μm, and therefore is comparable with the thickness of the metal plus photoresist layer stack (75 μm). This high aspect ratio entails poor control on the gaps profile producing over-etching and widening the spacing between dogbones. Indeed, as shown in [16], the magnetic resonance tends to increase slightly when the gap between dogbones is enlarged, which gives support to our hypothesis.

Fig. 16 shows the measured magnitude of the reflection coefficient for the complete antenna configuration including the HIS ("Complete antenna"), and the structure where the dogbone layer is replaced by a standard solid copper ground plane ("STD GND plane"). As apparent, the HIS contributes to significantly improve impedance matching and bandwidth performance.

Fig. 17 shows the normalized total field radiation pattern in the principal E and H planes of the dipole simulated using IE3D (with the finite size ground plane) versus measurements performed in our anechoic chamber facility. The simulated peak gain for each specific plane is 7.1 dBi in the H-plane, and 5.6 dBi in the E-plane, including all losses in the feed network, whereas maximum gain values of 6.4 dBi and 5.3 dBi were measured at 5.6 GHz (i.e. the measured resonance frequency) in the H plane and E-plane, respectively. A greater gain is obtained in the H plane because the maximum of radiation occurs at a slightly tilted angle with respect to the boresight direction. This small angle tilt in the H-plane is likely due to the coupling between the balun and the dipole and it is also observed in measurements. The patterns show that radiation in the forward direction is considerably increased with respect to the free-space dipole (providing a maximum directivity of 2.14 dBi). The radiation efficiency for this antenna was simulated to be 90% (IE3D), and measured to be 86% at 5.6 GHz by using the cylindrical Wheeler cap of diameter 90 mm and height 150 mm according to the measurement technique described in [27], [28].

VI. HIS Size Miniaturization Study

In order to study the effect of the HIS size on the antenna performance, simulation results relevant to the four structures shown in Fig. 18, differing for the number of unit cells the HIS is comprised of, namely 5×4, 5×2, 4×4 and 3×4 dogbone

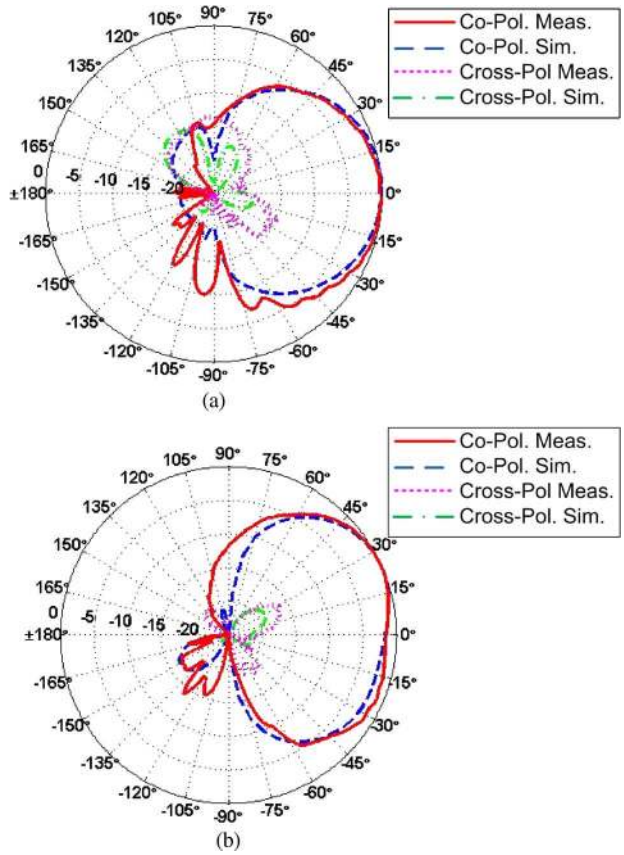

Fig. 17. Simulated and measured normalized total realized gain radiation patterns: (a) E- and (b) H-planes. Both copolar and cross-polar components are shown.

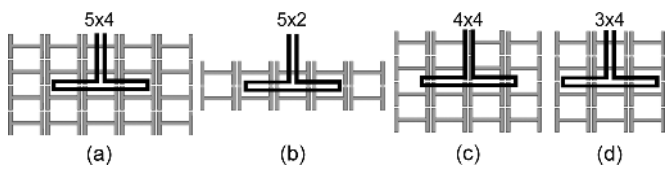

Fig. 18. Different sizes of HIS $M \times N$, where M and N denote dogbones columns and rows, respectively. (a) 5×4, (b) 5×2, (c) 4×4, and (d) 3×4.

unit cells, were compared to those obtained for the antenna with the original HIS (Fig. 11), formed by 5×6 unit cells. First we will consider the case that the number of unit cells is reduced while retaining an infinite ground plane underneath the dogbone layer. This case may apply when the antenna is placed on top of a large ground plane (e.g. when the antenna shares the ground plane with other system modules). For this case, the printed balun and all the other antenna dimensions are kept constant. Secondly, we will assume that the ground plane has the same finite size as the dogbone layer. In this case the balun structure could be larger than the relative ground, having the same size as the HIS, and therefore is not considered in the simulations, and the antenna is directly fed through the twin line. The presented results for the input resistance are referred to the folded dipole terminals by appropriate de-embedding. To our knowledge the HIS size reduction consideration has been only briefly commented on [8], [10] with two different HIS cases in terms of reflection coefficient. In this paper, a complete investigation

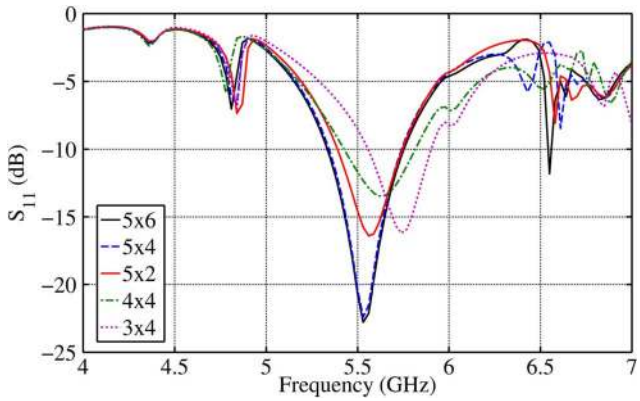

Fig. 19. Simulated reflection coefficient using Zeland IE3D for different HIS sizes.

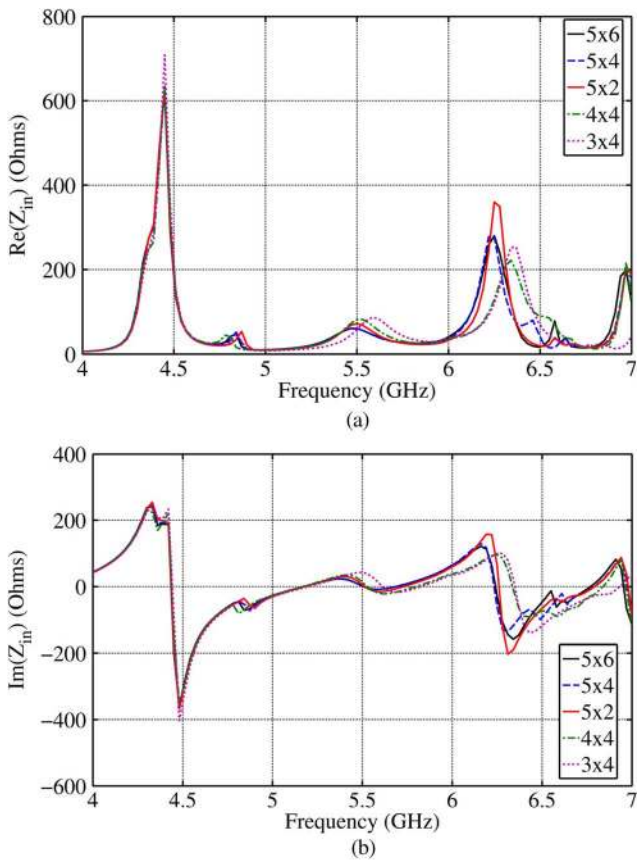

Fig. 20. (a) Real and (b) imaginary parts of the folded dipole input impedance simulated with Zeland IE3D for different HIS sizes.

of impedance, reflection coefficient, gain and radiation pattern is offered for multiple HIS sizes for finite and infinite ground plane cases.

A. Infinite Ground Plane

Fig. 19 shows the reflection coefficient of the five antenna configurations from Fig. 18 simulated under an infinite ground plane assumption, while in Fig. 20 are plotted the corresponding real and imaginary parts of the input impedance. Table I summarizes the relative −10 dB impedance bandwidths and peak gains for all considered HIS sizes. For the 5 × 4 dogbone array

TABLE I
RELATIVE BANDWIDTH AND PEAK GAINS FOR DIFFERENT HIS SIZES WITH INFINITE GROUND PLANE AT 5.5 GHz

HIS Size	5x	5x4	5x2	4x4	3x4
Relative Bandwidth (%)	8.2	8.1	6.5	7.4	6.1
Peak Gain (dBi)	7.3	7.2	7.0	7.1	6.8

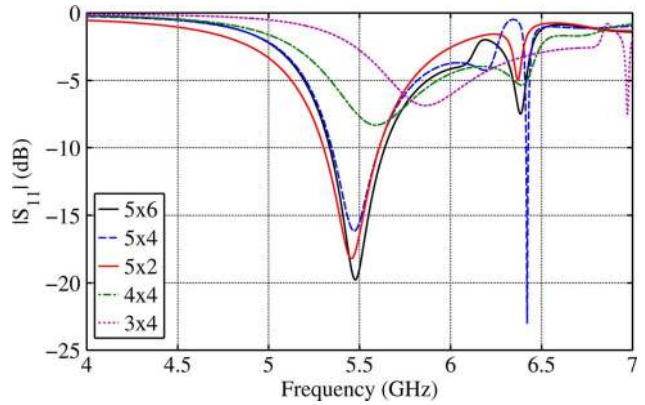

Fig. 21. Reflection coefficient of the folded dipole input impedance simulated with CST Microwave Studio for different HIS sizes. The reference impedance is 112 ohms (characteristic impedance twin line) due to the fact that the balun structure has been removed.

case, very small changes are observed in Fig. 19 for the bandwidth and resonant frequency, with respect to the 5 × 6 original HIS size. However, when the HIS size is further reduced, the resonant frequency shifts towards higher frequencies while the relative bandwidth reduces.

The simulated relative bandwidth and peak gains for all considered configurations are summarized in Table I. For the HISs smaller than the original size, a slight reduction of the maximum gain is observed in both the E- and H-planes. With respect to the radiation pattern shape very little variation was observed between the different HIS sizes. This experiment shows that the impact of reducing the HIS size over the frequency and antenna gain is limited if a large ground plane is available.

B. Finite Ground Plane

We now consider the case when the ground plane has the same finite size as the dogbone layer. As mentioned above, in this case the balun structure is not considered in the simulations. The reflection coefficient and input impedance de-embedded to the folded dipole terminals for variable HIS and ground plane sizes are shown in Fig. 21 and Fig. 22, respectively. In this case, the antenna impedance matching varies significantly with the HIS size, contrarily to the infinite ground plane case.

More precisely, when the size of the HIS is reduced from the original 5 × 6 unit cells to 5 × 4 and 5 × 2 unit cells, the reflection coefficient changes slightly and the dipole remains impedance matched to the twin line. Instead, the matching noticeably deteriorates when the HIS is reduced to 4 × 4 and 3 × 4 unit cells. Indeed, in these latter cases the dipole input resistance significantly decreases, and not even by adjusting the dipole length the antenna can any longer be matched to the twin line impedance. In fact, varying the dipole length changes

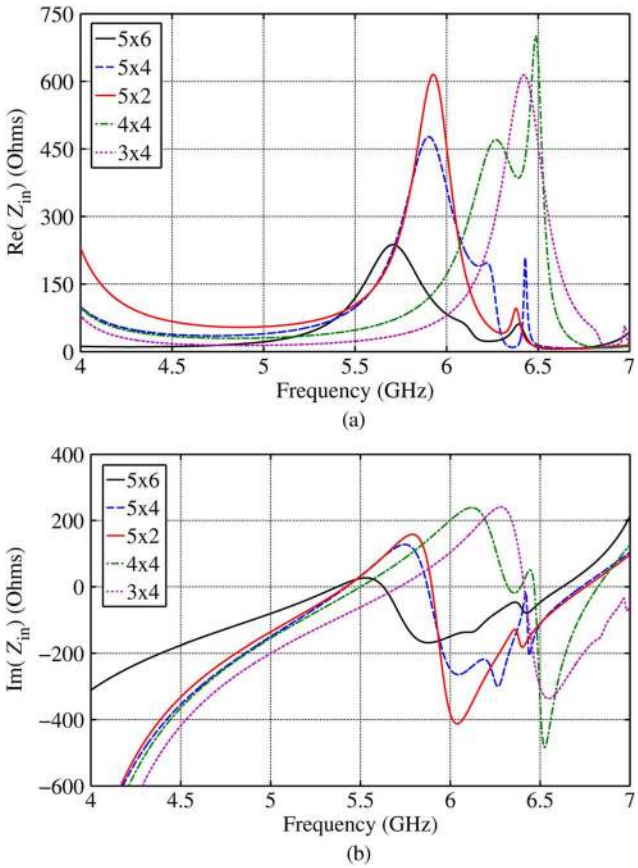

Fig. 22. (a) Real and (b) imaginary parts of the folded dipole input impedance simulated with CST Microwave Studio for different HIS sizes.

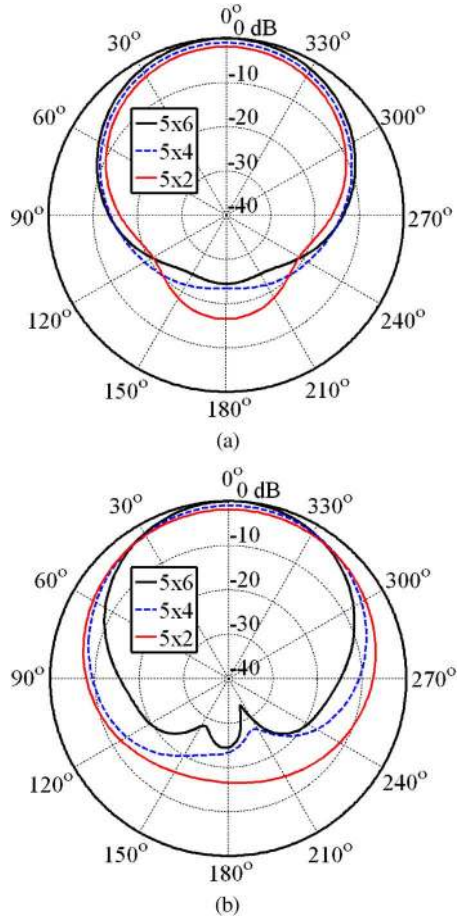

Fig. 23. Simulated normalized total gain radiation patterns 5.5 GHz of the antennas in Fig. 18 with finite ground plane: (a) E- and (b) H-planes for different HIS sizes.

the imaginary part of the input impedance and the frequency where it goes to zero (resonance), but it does not provide the larger values of the input resistance at the resonance required to impedance matching the antenna with the smaller HISs. On the other hand, due to the absence of the balun structure, the additional resonance shown in Fig. 20(b) around 4.5 GHz does not appear in Fig. 22(b).

Next we examine the radiation performance of those finite size HIS antenna configurations exhibiting a good impedance matching and low reflection coefficient at the desired operating frequency. Fig. 23 shows the radiation patterns simulated by CST at 5.5 GHz for the folded dipole with the 5×6, 5×4 and 5×2 HISs, assuming the relative ground planes to have the same finite size as the different dogbone layers above it. Some reduction of the gain is observed when the HIS size decreases and back radiation level increases. Having removed the balun structure, pattern tilting appears to be negligible.

Peak gains, relative bandwidths, and radiation efficiencies associated to the selected antenna configurations are summarized in Table II. Though for increasingly smaller HISs obviously the gain and radiation efficiency progressively reduces, it can be noted that even the smallest HIS provides considerably improved performance both in terms of peak gain with respect a free-space dipole (2.14 dBi) and impedance bandwidth with respect to both configurations examined in Section II that include a PEC, PMC (Fig. 3), or a grounded dielectric slab (Fig. 5) as reflecting surfaces.

TABLE II
RELATIVE BANDWIDTHS, PEAK GAINS AND RADIATION EFFICIENCIES, FOR DIFFERENT HIS SIZES WITH FINITE GROUND PLANE AT 5.5 GHz

HIS Size	5x6	5x4	5x2
Relative Bandwidth (%)	5.6	4.84	5.64
Peak Gain (dBi)	7.75	6.73	5.83
Radiation efficiency (%)	94	91	83

As a final remark, from the above simulation results we conclude that too small HISs tend to give input resistance values much lower than required to match the dipole to the twin line impedance ($\sim$112 Ohms), and increasingly smaller gains. Practically, to achieve good impedance matching and gain performance, the HIS is required to extend all around the dipole for at least one row/column of unit cells.

VII. CONCLUSIONS

In this work, the advantages of using high impedance surfaces over other potential solutions for the design of low profile dipole antennas have been remarked. It has been shown that by using a HIS, a low profile antenna (in the z direction), with directional pattern and higher impedance bandwidth than a dipole in front of a PEC can be achieved.

We have presented simulation and measurement results of a fully planar realization of a low profile dipole antenna and

a comprehensive explanation of the HIS characteristics. The paper shows a working prototype and we show that the total surface area realized here could be miniaturized up to some extent. The measured magnitude of the reflection coefficient (< -15 dB) and measured gain (6.4 dBi) confirm the good performance of our prototype and prove that the developed concept can be used to design antennas with miniaturized thickness in fully planar technology.

This kind of low profile antennas also offer viable solutions for vehicle, naval, and aerospace platforms, for integrating a conformal efficient antenna system on top of pre-existing metal structure.

ACKNOWLEDGMENT

The authors acknowledge Rogers Corporation for providing them with the substrate material used to fabricate the antenna. They also thank Mentor Graphics Corporation (IE3D), Computer Simulation Technology (CST) and Ansoft HFSS for providing the simulation tools that were instrumental in the design process. Final thanks go to C. Guclu and J. Sloan, at the University of California Irvine, for their valuable input and discussions.

REFERENCES

[1] D. Sievenpiper, L. Zhang, R. F. Jimene Broas, N. G. Alexopolous, and E. Yablonovitch, "High-impedance electromagnetic surfaces with a forbidden frequency band," *IEEE Trans. Microwave Theory Tech.*, vol. 47, no. 11, pp. 2059–2074, Nov. 1999.

[2] N. G. Alexopoulos, H. Contopanagos, and C. Kyriazidou, "Method of Generating a Magnetic Interface," U.S. Patent 7109947B2, 2000.

[3] N. G. Alexopoulos, H. Contopanagos, and C. Kyriazidou, "Inductor Circuit With a Magnetic Interface," U.S. Patent 7116202B2, 2000.

[4] N. G. Alexopoulos, F. De Flaviis, and Y. Liu, "KCA elements in electromagnetically metamorphic objects and interfaces," in *Proc. Union Radio-Scientifique Internationale (URSI) Symp. on Electromagn. Theory*, Pisa, Italy, 2004, pp. 688–690.

[5] C. R. Simovski, P. D. Maagt, and I. V. Melchakova, "High-impedance surfaces having stable resonance with respect to polarization and incidence angle," *IEEE Trans. Antennas Propag.*, vol. 53, no. 3, pp. 908–914, Mar. 2005.

[6] N. G. Alexopoulos, H. Contopanagos, and C. Kyriazidou, "Antenna With a Magnetic Interface," U.S. Patent 6853350B2, 2000.

[7] F. Yang and Y. Rahmat-Samii, "Reflection phase characterizations of the EBG ground plane for low profile wire antenna applications," *IEEE Trans. Antennas Propag.*, vol. 51, no. 10, pp. 2691–2703, Oct. 2003.

[8] L. Akhoondzadeh-Asl, D. J. Kern, P. S. Hall, and D. H. Werner, "Wideband dipoles on electromagnetic bandgap ground planes," *IEEE Trans. Antennas Propag.*, vol. 55, no. 9, pp. 2426–2434, Sept. 2007.

[9] H. Mosallaei and K. Sarabandi, "Antenna miniaturization and bandwidth enhancement using a reactive impedance substrate," *IEEE Trans. Antennas Propag.*, vol. 52, no. 9, pp. 2403–2414, Sep. 2004.

[10] S. R. Best and D. L. Hanna, "Design of broadband dipole in close proximity to an EBG ground plane," *IEEE Antennas Propag. Mag.*, vol. 50, no. 6, pp. 52–64, 2008.

[11] A. Vallecchi and F. Capolino, "Thin high-impedance metamaterial substrate and its use in low profile antennas suitable for system integration," in *Proc. 59th Electronic Components and Technology Conf. (ECTC)*, May 2009, pp. 777–783.

[12] A. Vallecchi, M. Albani, and F. Capolino, "Planar metamaterial transverse equivalent network and its application to low-profile antenna designs," in *Proc. Eur. Conf. on Antennas and Propagation (EUCAP)*, Berlin, Germany, Mar. 23–27, 2009, pp. 861–865.

[13] G. Donzelli, A. Vallecchi, F. Capolino, and A. Schuchinsky, "Anisotropic metamaterial made of paired planar conductors: Particle resonances, phenomena and properties," *Metamaterials (Elsevier)*, vol. 3, no. 1, pp. 10–27, 2009.

[14] F. Yang, V. Demir, D. A. Elsherbeni, A. Z. Elsherbeni, and A. A. Eldek, "Planar dipole antennas near the edge of an EBG ground plane," in *Proc. Antennas and Propag Symp.*, Jul. 2005, vol. 1A, pp. 750–753.

[15] M. Z. Azad and M. Ali, "Novel wideband directional dipole antenna on a mushroom like EBG structure," *IEEE Trans. Antennas Propag.*, vol. 56, no. 5, May. 2008.

[16] A. Vallecchi, F. Capolino, and A. Schuchinsky, "2-D Isotropic effective negative refractive index metamaterial in planar technology," *IEEE Microw. Wireless Comp. Lett.*, vol. 19, no. 5, pp. 269–271, 2009.

[17] A. Vallecchi and F. Capolino, "Metamaterials based on pairs of tightly-coupled scatterers," in *Theory and Phenomena of Metamaterials*. Boca Raton, FL: CRC Press, 2009, ch. 19.

[18] A. Vallecchi and F. Capolino, "Tightly coupled tripole conductor pairs as constituents for a planar 2D-isotropic negative refractive index metamaterial," *Opt. Express*, vol. 17, no. 17, pp. 15216–15227, 2009.

[19] A. Vallecchi, F. Capolino, J. De Luis, and F. De Flaviis, "A low profile folded dipole antenna on a reactive high impedance substrate," presented at the Int. Conf. on Electromagnetics in Advanced Applications (ICEAA 2009), Torino, Italy, Sep. 14–18, 2009.

[20] A. Vallecchi, F. Capolino, and M. Albani, "Metamaterial made of pairs of conductors in planar technology: A Z-transmission line approach," presented at the Metamaterials Conf., Pamplona, Spain, Sep. 21–26, 2008.

[21] S. R Best, "Improving the performance properties of a dipole element closely spaced to a PEC ground plane," *IEEE Antennas Wireless Propag. Lett.*, vol. 3, 2004.

[22] G. A. Thiele, E. P. Ekelman, Jr, and L. W. Henderson, "On the accuracy of the transmission line model for the folded dipole," *IEEE Trans. Antennas Propag.*, vol. 28, no. 5, pp. 700–703, Sep. 1980.

[23] J. S. Lim, H. S. Yang, Y. T. Lee, S. Kim, K. S. Seo, and S. Nam, "E-Band Wilkinson balun using CPW MMIC technology," *Electron. Lett.*, vol. 40, no. 14, Jul. 2004.

[24] E. J. Wilkinson, "An N-way hybrid power divider," *IRE Trans. Microw. Theory Technol.*, vol. MTT-8, pp. 116–118, 1960.

[25] Y. Qian and T. Itoh, "A broadband microstrip-to-CPS transition," in *Asia Pacific Microwave Conf. Dig.*, Hong Kong, 1997, pp. 609–612.

[26] R. J. P. Douville and D. S. James, "Experimental study of symmetric microstrip bends and their compensation," *IEEE Trans. Microw. Theory Tech.*, vol. MTT-26, pp. 175–181, Mar. 1978.

[27] R. H. Johnston and J. G. McRory, "An improved small antenna radiation-efficiency measurement method," *IEEE Antennas Propag. Mag.*, vol. 40, pp. 40–48, 1998.

[28] C. Mendes and C. Peixeiro, "Radiation efficiency of several handset antennas obtained with a modified wheeler cap method," in *Proc. 2nd Eur. Conf. on Antennas and Propagation, EuCAP*, 2007, pp. 1–4.

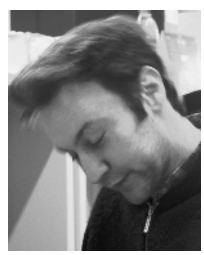

Andrea Vallecchi received the Laurea (M.Sc) degree (*summa cum laude*) in electronic engineering from the University of Florence, Florence, Italy, and the Ph.D. degree in information engineering, applied electromagnetics, and telecommunications from the University of Salerno, Salerno, Italy.

He then worked at the Laboratory of Antennas and Microwaves. University of Florence, as a Research Associate, and subsequently, since 2007, has been a Postdoctoral Research Fellow at the University of Siena. In 2009, he spent some months working as an Assistant Specialist at the University of California, Irvine. In 2009 and 2010, he was a Visiting Researcher at Queen's University of Belfast, Belfast, U.K. He is currently with the Department of Information Engineering, University of Siena. His present research interests are in the theoretical characterization and design of metamaterials for applications at microwaves and visible frequencies.

Javier R. De Luis (S'08–M'11) was born in Elche, Spain, in 1982. He received the Telecommunication Engineer degree from the Universitat Politècnica de Catalunya (UPC), Barcelona, Spain and the M.S. degree from the University of California at Irvine (UCI) in 2008, where he is currently working toward the Ph.D. degree.

His current research is focused on reconfigurable antennas for tunable RF handset front end and smart systems.

Filippo Capolino (S'94–M'97–SM'04) received the Laurea (*cum laude*) and Ph.D. degrees in electrical engineering from the University of Florence, Italy, in 1993 and 1997, respectively.

He is presently employed as an Assistant Professor at the Department of Electrical Engineering and Computer Science, University of California, Irvine. He has been an Assistant Professor at the Department of Information Engineering, University of Siena, Italy. During 1997–1999, he was a Postdoctoral Fellow with the Department of Aerospace and Mech. Engineering, Boston University, MA. From 2000 to 2001 and in 2006, he was a Research Assistant Visiting Professor with the Department of Electrical and Comp. Engineering, University of Houston, TX. His research interests include antennas, metamaterials and their applications, sensors in both microwave and optical ranges, wireless systems, chip-integrated antennas. He has been the EU Coordinator of the EU Doctoral Programs on Metamaterials (2004–2009).

Dr. Capolino received several Young and Senior Scientist Travel Grants to attend international conferences (IEEE and URSI) and two Student and Young Scientist Paper Competition Awards. In 2000, he received the R.W. P. King Prize Paper Award from the IEEE Antennas and Propagation Society for the Best Paper by an author under 36. He is a coauthor of "Fast Breaking Papers, Oct. 2007" in EE and CS, about metamaterials (paper that had the highest percentage increase in citations in Essential Science Indicators, ESI). In 2002–2008, he served as an Associate Editor for the IEEE TRANSACTIONS ON ANTENNAS AND PROPAGATION. Since 2007, he is a founder and an Editor of the new Elsevier journal *Metamaterials*. He is the Editor of the *Metamaterials Handbook*, CRC-Press, 2009.

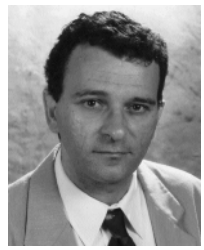

Franco De Flaviis (SM'07) was born in Teramo, Italy, in 1963. He received the Laurea degree in electronics engineering from the University of Ancona (Italy), in 1990, and the M.S. and Ph.D. degrees in electrical engineering from the University of California at Los Angeles (UCLA), in 1994 and 1997, respectively.

In 1991, he was an Engineer at Alcatel, where his research specialized in the area of microwave mixer design. In 1992, he was Visiting Researcher at UCLA working on low intermodulation mixers. He is currently a Professor with the Department of Electrical Engineering and Computer Science, University of California, Irvine. He has authored and coauthored over 100 papers in refereed journals and conference proceedings, filed several international patents and authored one book and three book chapters. His research interests include the development of microelectromechanical systems (MEMS) for RF applications fabricated on unconventional substrates, such as printed circuit board and microwave laminates with particular emphasis on reconfigurable antenna systems. He is also active in the research field of highly integrated packaging for RF and wireless applications.

Dr. De Flaviis is a member of URSI Commission B.